

# SPUD: Simultaneous Phase Unwrapping and Denoising Algorithm for Phase Imaging

JESUS PINEDA<sup>1</sup>, JORGE BACCA<sup>2</sup>, JHACSON MEZA<sup>1</sup>, LENNY A. ROMERO<sup>3</sup>, HENRY ARGUELLO<sup>2</sup>, AND ANDRES G. MARRUGO\*<sup>1</sup>

<sup>1</sup> Facultad de Ingeniería, Universidad Tecnológica de Bolívar, Cartagena, Colombia

<sup>2</sup> Department of Computer Science, Universidad Industrial de Santander, Bucaramanga, Colombia

<sup>3</sup> Facultad de Ciencias Básicas, Universidad Tecnológica de Bolívar, Cartagena, Colombia

\* Corresponding author: agmarrugo@utb.edu.co

Compiled July 22, 2021

Recent methods for phase unwrapping in the presence of noise include denoising algorithms to filter out noise as a pre-processing stage. However, including a denoising stage increases the overall computational complexity resulting in long execution times. In this paper, we present a non-iterative Simultaneous Phase Unwrapping and Denoising algorithm for phase imaging, referred to as SPUD. The proposed method relies on the least-squares Discrete Cosine Transform (DCT) solution for phase unwrapping with an additional sparsity constraint on the DCT coefficients of the unwrapped solution. Simulation results with different levels of noise and wrapped phase fringe density reveal the suitability of the proposed method for accurate phase unwrapping and restoration. When compared to the 2D windowed Fourier transform filter, SPUD performs better in terms of phase error and execution times. The processing of experimental data from synthetic aperture radar showed the capability for processing real images, including removing phase dislocations. An implementation of the proposed algorithm can be accessed and executed through a Code Ocean compute capsule.

© 2021 Optical Society of America

<http://dx.doi.org/10.1364/ao.XX.XXXXXX>

## 1. INTRODUCTION

Two-dimensional (2D) phase unwrapping is a necessary process in many applications such as synthetic radar aperture, fringe projection profilometry, interferometry, magnetic resonance imaging, among others [1–3]. The unwrapping process consists in retrieving the continuous phase  $\varphi$  from its wrapped version  $\psi$ , which lies in the interval  $(-\pi, \pi]$  [4]. In the noiseless scenario, phase unwrapping is trivial and straightforward. However, in practice,  $\psi$  is affected by noise, which makes phase unwrapping difficult and decreases the measurement accuracy [5, 6].

Phase unwrapping has been traditionally approached from two perspectives [7]. In the classical approach, the goal is to obtain a continuous phase regardless of the presence of noise. Conventional phase unwrapping algorithms such as path-following approaches [8], quality-guided path-following methods [9, 10], mask-cut phase unwrapping [11], Flynn's minimum discontinuity [12], and minimum  $L^p$ -norm algorithms [1, 13], follow this perspective [1, 14]. Quality-guided and  $L^p$ -norm phase unwrapping algorithms have shown the best performance in the

presence of low-level noise [1], although the computation of quality maps increases the complexity [15]. Recently, an iterative least-squares-based phase unwrapping method referred to as CPULSI [16] has proven to be highly suitable even on extremely noisy phases [5]. However, despite obtaining an accurate continuous phase map, a further denoising stage must be applied to estimate a phase map suitable for quantitative measurements [5, 17].

The second perspective includes denoising preprocessing stages to produce a restored wrapped phase map, followed by phase unwrapping. For instance, Montresor and Picart [18] evaluated the performance of state-of-the-art algorithms for phase data denoising including Wiener filtering [19, 20], Wavelet thresholding approaches [21, 22], non-local means [23–25], transform-based block-matching 3D (BM3D) filter [26, 27], 2D windowed Fourier transform filter (WFF) [10, 28, 29], and the SPADEDH algorithm [30, 31]. They quantitatively assessed these algorithms and ranked them according to their performance to isolate the genuine phase gradients from the noisy wrapped

phase. In terms of phase errors, WFF outperformed the evaluated methods, followed by the Curvelet Decomposition method, especially when the noise level is high. Recently, Krishnan et al. [32] proposed a multi-resolution windowed Fourier analysis for interferometric phase denoising, referred to as SURE-fuse WFF. This method proved to outperform its fixed resolution WFF counterpart. The second perspective has proven to be more effective for phase data restoration than combining perspective 1 with a further denoising stage [5]. However, most of the denoising algorithms are of parametric and interactive nature, which could result in time-consuming tunable methods with high computational complexity and long execution times. Also, when both noise and fringe densities are high, prefiltering may lead to phase dislocations [16, 17, 33].

An additional third perspective involves simultaneous unwrapping and denoising. For example, Marroquin and Rivera [34] proposed a phase unwrapping algorithm that relies on a generalized least-squares solution with Tikhonov regularization. The introduction of the regularization term resulted in the reduction of noise and the estimation of missing data regions. Similarly, Guerriero et al. [35] proposed a regularization scheme for solving the phase unwrapping as a constrained optimization problem for a vector field of integers. More recently, Zhuo et al. [36] proposed a sparse Markov random field approach for phase unwrapping of Interferometric synthetic aperture radar (InSAR) data. This perspective is highly suitable for phase unwrapping in the presence of noise and missing data regions. However, these methods use iterative procedures to obtain the solution, which could result in long execution times.

In this paper, we propose a Simultaneous Phase Unwrapping and Denoising algorithm for phase imaging, referred to as SPUD. The method solves the least-squares phase differences using the Discrete Cosine Transform (DCT) closed solution combined with a hard-thresholding operation. The method exploits the fact that the correct phase can be sparsely represented in the DCT domain. Unlike the methods in the third perspective, SPUD is a non-iterative algorithm with a computational complexity of  $\mathcal{O}(N \log N)$ , which allows a fast phase restoration compared to existing iterative methods. Least-squares solutions for phase unwrapping have been widely used in the literature [1, 2, 37]. However, despite their success, often, the unwrapped phase still has noise. Several authors have proposed an additional denoising stage [37], but this increases the complexity of the method, which is its main appeal.

## 2. PROBLEM FORMULATION

The goal in 2D phase unwrapping is to estimate the true phase image  $\phi \in \mathbb{R}^{M \times N}$ , from a wrapped phase image  $\psi \in (-\pi, \pi]^{M \times N}$  defined by

$$\psi = \mathcal{W}\{\phi\}, \quad (1)$$

where  $\mathcal{W}\{\cdot\}$  is the wrapping operator that performs component-wise  $2\pi$  modulo wrapping operation

$$\begin{aligned} \mathcal{W} &= : \mathbb{R}^{M \times N} \rightarrow (-\pi, \pi]^{M \times N}, \\ \psi &\rightarrow \text{mod}(\phi + \pi, 2\pi) - \pi. \end{aligned} \quad (2)$$

The proposed formulation relies on two assumptions. The first is that the desired unwrapped phase and the wrapped phase have the same local phase differences. Therefore, it is conventional to define

$$\Delta\psi_{i,j}^x = \mathcal{W}\{\psi_{i+1,j} - \psi_{i,j}\}, \quad \Delta\psi_{i,j}^y = \mathcal{W}\{\psi_{i,j+1} - \psi_{i,j}\}, \quad (3)$$

as the horizontal and vertical phase differences, respectively. This assumption has an exact solution by solving a least-squares algorithm (in the noiseless scenario) [1, 13] or shows desirable results when the noise present in the differences does not exceed  $\pi$ , i.e.,  $|\psi_{i+1,j} - \psi_{i,j} + \eta_{i,j}| < \pi$ , where  $\eta_{i,j}$  is the noise of the horizontal differences. It occurs similarly for vertical differences. The second assumption of this work is that the true phase image is smooth [38]. Therefore, it can be sparsified in a given transformation  $\mathcal{T}(\cdot)$ , i.e.,  $\|\mathcal{T}(\phi)\|_0 = k \ll MN$ , where  $\|\mathbf{x}\|_0 = |\{i : x_i \neq 0\}|$  with  $|\{\cdot\}|$  as the cardinality of a set, such that, the  $\ell_0$ -norm counts the number of nonzero elements of  $\mathbf{x}$ . Additionally, in a noisy phase image, the sparsity property implies that the relevant information is concentrated in few coefficients, while the power of the noise remains white [39]. Hence, a least-squares phase unwrapping formulation incorporating these two assumptions can be expressed as

$$\min \left\{ \sum_{ij} (\Delta\phi_{i,j}^x - \Delta\psi_{i,j}^x)^2 + \sum_{ij} (\Delta\phi_{i,j}^y - \Delta\psi_{i,j}^y)^2 \right\} + \|\mathcal{T}(\phi)\|_0, \quad (4)$$

where  $\Delta\phi_{i,j}^x$  and  $\Delta\psi_{i,j}^x$  denote the  $x$ -components of the unwrapped and wrapped phase gradients, respectively;  $\Delta\phi_{i,j}^y$  and  $\Delta\psi_{i,j}^y$  are their  $y$ -components counterparts.

## 3. PROPOSED METHOD

In this work, we propose a non-iterative method to solve Eq. (4). In particular, notice that the left side of Eq. (4) is reduced to the Hunt's matrix formulation given by,

$$(\phi_{i+1,j} - 2\phi_{i,j} + \phi_{i-1,j}) + (\phi_{i,j+1} - 2\phi_{i,j} + \phi_{i,j-1}) = \rho_{i,j}, \quad (5)$$

where,

$$\rho_{i,j} = (\Delta\psi_{i,j}^x - \Delta\psi_{i-1,j}^x) + (\Delta\psi_{i,j}^y - \Delta\psi_{i,j-1}^y). \quad (6)$$

Additionally, Eq. (6) can be interpreted as the discretization of the Poisson's equation with Neumann boundary conditions

$$\nabla^2 \phi_{i,j} = \rho_{i,j}, \quad (7)$$

where  $\nabla^2$  is the Laplacian operator. Therefore, applying the two-dimensional DCT on the  $M \times N$  grid to both sides of Eq. (7) yields

$$\hat{\phi}_{i,j} = \frac{\hat{\rho}_{i,j}}{2[\cos(\pi i/M) + \cos(\pi j/N) - 2]}, \quad (8)$$

where  $\hat{\phi}_{i,j} = \mathcal{T}(\phi_{i,j})$  and  $\hat{\rho}_{i,j} = \mathcal{T}(\rho_{i,j})$  denote the 2-D forward DCT of  $\phi_{i,j}$  and  $\rho_{i,j}$ , respectively. The sparsity information can be exploited using the element-wise hard-thresholding operator  $\Theta_{hard}^\lambda(\cdot)$ , which can be directly applied in the sparse vector to reduce the noise [39], i.e, in the DCT domain defined as

$$\Theta_{hard}^\lambda(\hat{\phi}_{i,j}) = \begin{cases} 0 & \text{if } |\hat{\phi}_{i,j}| \leq \lambda \\ \hat{\phi}_{i,j} & \text{otherwise} \end{cases}. \quad (9)$$

Finally, the noise-free solution  $\phi_{i,j}$  is obtained by the inverse DCT of Eq. (9), i.e.,  $\phi = \mathcal{T}^{-1}(\Theta_{hard}^\lambda(\hat{\phi}_{i,j}))$ . Notice that the

mean squared error (MSE) of the true phase and the thresholded estimation (Eq. (9)), can be written as

$$\begin{aligned} \mathbb{E} \left[ \left\| \phi - \mathcal{T}^{-1} \left( \Theta_{hard}^{\lambda}(\hat{\phi}_{i,j}) \right) \right\|_2^2 \right] = \\ \sum_{i,j: |\hat{\phi}_{i,j}| \leq \lambda} \left| \mathcal{T}(\phi_{i,j}) \right|^2 + \sigma^2 \left| \{i,j : |\hat{\phi}_{i,j}| > \lambda\} \right|, \end{aligned} \quad (10)$$

where the first and second terms are, respectively, the bias and the variance of the thresholded estimation, assuming Gaussian white noise with variance  $\sigma^2$ . Additionally, with a threshold parameter  $\lambda$  sufficiently close to  $\sigma \sqrt{2 \log(MN)}$ , the MSE is close to that of an oracle projection, which reduces the variance without increasing the bias, resulting in an optimal denoising value [40]. Algorithm 1 summarizes the steps explained above.

#### Algorithm 1. SPUD: Simultaneous Phase Unwrapping and Denoising Algorithm for Phase Imaging

- 1: **Input:** Wrapped phase image  $\psi$  and the threshold parameter  $\lambda$ .
- 2: **Method:**
- 3:  $\rho_{i,j} = (\Delta\psi_{i,j}^x - \Delta\psi_{i-1,j}^x) + (\Delta\psi_{i,j}^y - \Delta\psi_{i,j-1}^y)$  .
- 4:  $\hat{\rho} = \mathcal{T}(\rho)$  ▷ DCT transform
- 5:  $\hat{\phi}_{i,j} = (\hat{\rho}_{i,j}) / 2[\cos(\pi i/M) + \cos(\pi j/N) - 2]$
- 6:  $\hat{\phi}_{i,j} = \Theta_{hard}^{\lambda}(\hat{\phi}_{i,j})$  ▷ Hard-thresholding operator
- 7: **Output:** Restored phase  $\phi = \mathcal{T}^{-1}(\hat{\phi})$

#### A. Computational complexity

One of the main advantages of the proposed method is its low computational complexity since it is a non-iterative algorithm. Following the SPUD algorithm steps, it can be observed that the DCT transform has a computational complexity of  $\mathcal{O}(N \log N)$  and the hard-threshold of  $\mathcal{O}(N)$ . Therefore, the SPUD algorithm has a computational complexity of  $\mathcal{O}(N \log N)$ .

#### 4. SIMULATIONS FOR PERFORMANCE ASSESSMENT

The performance of the proposed method was evaluated with numerically simulated data and compared to a denoising plus phase unwrapping strategy from the second perspective described in the introduction. The denoising stage is performed using the 2D Windowed Fourier Transform filter (WFF) [10, 28, 29], which was shown to outperform the state-of-the-art denoising algorithms in terms of phase error [18]. For the phase unwrapping stage, we used the least-squares DCT closed solution. This method is referred to from now on as WFF+LSPU. We used the suggested parameter settings for WFF provided in [10].

The motivation for these experiments is to find out if for mild phase noise can the costly WFF be avoided with an alternative and simpler approach such as the hard-thresholding in the DCT domain while simultaneously carrying out phase unwrapping. For this reason, we do not compare against other noise-robust phase unwrapping methods, like PUMA [41], that have been shown to require additional denoising stages [42].

#### A. Data-set

The data-set was generated from five  $256 \times 256$  reference phases (i.e., true phases) using the MATLAB® peaks function which provides progressive peak-to-valley values. From each reference phase, we generated 20 noise levels, i.e., 20 noisy wrapped phase

maps with uniformly distributed random noise with progressive standard deviations  $\sigma$  in the interval  $0.1 \leq \sigma \leq 0.5$ . We consider low to mild noise levels because higher noise levels increase rapidly the amount of residues in the wrapped phase [43, 44], which require more computationally demanding methods that deal directly with phase residues. In Fig. 1, we show ten of these phase maps, which summarizes the five fringe densities and the noise levels 1 and 20. Summing up, there were 100 noisy wrapped phase maps, which offers a comprehensive phase map diversity to produce statistics. The threshold parameter for these simulations was chosen according to  $\lambda = \sigma \sqrt{2 \log(MN)}$ .

#### B. Performance assessment

The performance assessment was carried out using three metrics. The first is the standard deviation of the restored phase error, which is given by [18],

$$\sigma_{\epsilon} = \sqrt{\mathbb{E} [\epsilon^2] - \mathbb{E} [\epsilon]^2}, \quad (11)$$

where  $\epsilon = \varphi_s - \varphi_r$  is the phase difference between the simulated true phase  $\varphi_s$ , and the restored phase map  $\varphi_r$ .  $\mathbb{E} [\cdot]$  denotes the expected value. Since the aim of phase restoration is related to metrology purposes, the standard deviation of phase error is an important parameter. Ideally, if the evaluated algorithm does not introduce errors, the simulated phase should be equal to the restored phase.

The second metric is called the *Quality Index* and models the phase degradation as structural distortions instead of errors [46]. The Quality Index is defined as,

$$Q_{index} = \frac{\sigma_{sr}}{\sigma_s \sigma_d} \cdot \frac{2\mu_s \mu_r}{\mu_s^2 + \mu_r^2} \cdot \frac{2\sigma_s \sigma_r}{\sigma_s^2 + \sigma_r^2}, \quad (12)$$

where  $\mu_s$  and  $\mu_r$  denote the mean values of the simulated true phase and the restored phase map, respectively.  $\sigma_s$  and  $\sigma_r$  are their variances and  $\sigma_{sr}$  the covariance. The value of  $Q_{index}$  is defined to lie in the interval  $[-1, 1]$ , being 1 a perfect similarity.

The third metric is the peak-signal-to-noise ratio (PSNR), and it is mostly related to the denoising performance. The PSNR between  $\varphi_s$  and  $\varphi_r$  is defined by

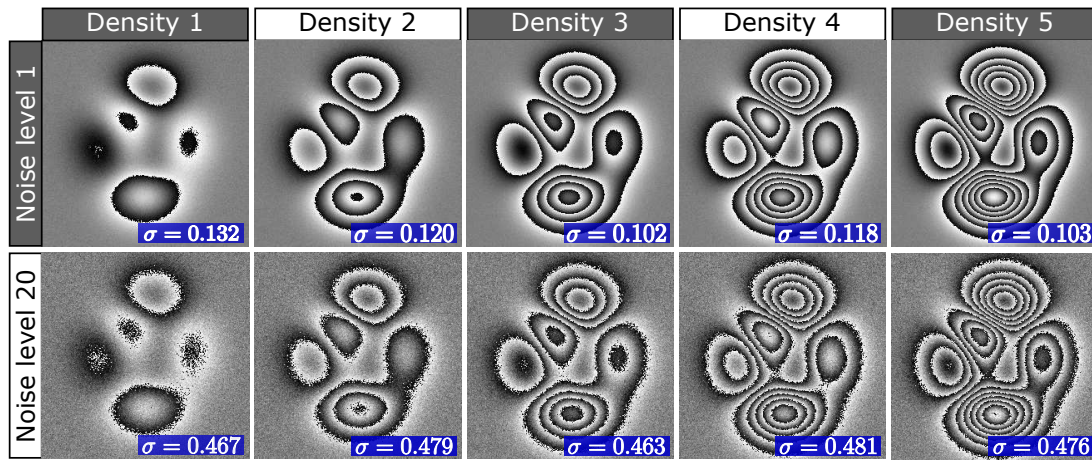
$$PSNR = 10 \cdot \log_{10} \left( \frac{\|\varphi_s\|_{\infty} M N}{\|\varphi_r - \varphi_s\|_F^2} \right), \quad (13)$$

where  $\|\varphi_r\|_{\infty}$  denotes the maximum input value of  $\varphi_r$ ;  $\|\cdot\|_F$  is the Frobenius norm and  $M, N$  are the number of rows, and columns, respectively.

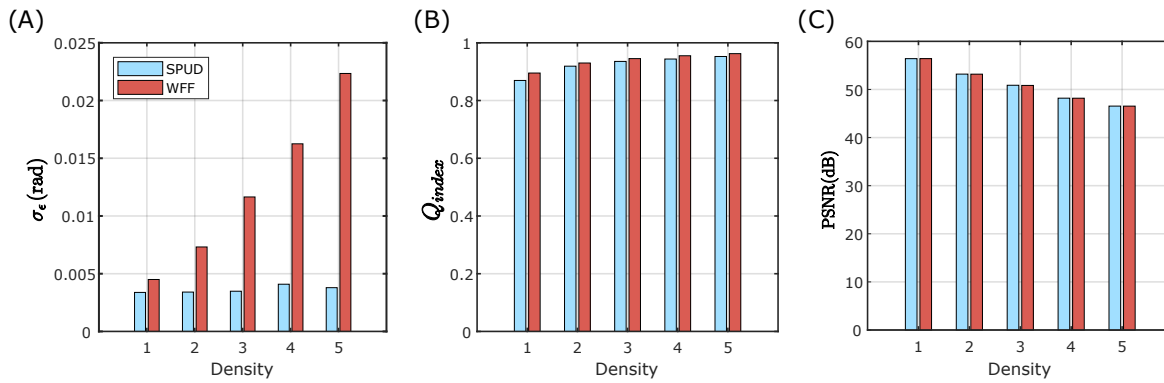
#### C. Simulation results and discussion

Fig. 2 summarizes the performance of the SPUD algorithm and WFF+LSPU for the entire dataset and the three metrics explained above. We plot the average values of  $\sigma_{\epsilon}$ ,  $Q_{index}$ , and PSNR for the 20 simulated noise levels at each fringe density. From Fig. 2 (A), the proposed method showed the best performance in terms of phase errors compared to WFF+LSPU regardless of fringe density. Whereas from Figures 2 (B) and (C), the SPUD method performs at par with respect to WFF+LSPU in terms of  $Q_{index}$  and PSNR.

To visualize the performance results, in Fig. 3, we summarize the outputs from the SPUD algorithm and WFF+LSPU for the different five phase densities and the highest noise level. Both methods effectively reduced the noise and correctly unwrapped the phase. However, the phase errors obtained by the proposed



**Fig. 1.** Simulated wrapped phase maps for the five fringe densities and the noise levels 1 and 20.



**Fig. 2.** Average phase restoration performance results of SPUD and WFF+LSPU. SPUD outperforms WFF+LSPU in terms of (A) restored phase error ( $\sigma_\epsilon$ ), and performs at par with WFF+LSPU in terms of (B) Quality index and (C) PSNR.

**Table 1.** Quantitative assessment of the phase estimation quality in Fig. 3. In bold typeface the values where SPUD performance is superior.

Density	$\sigma$	SPUD			WFF + LSPU		
		$\sigma_\epsilon$ (rad)	$Q_{index}$	PSNR (dB)	$\sigma_\epsilon$ (rad)	$Q_{index}$	PSNR (dB)
1	0.467	0.0059	0.838	56.33	0.0057	0.849	56.36
2	0.479	<b>0.0067</b>	0.878	<b>53.21</b>	0.0092	0.899	53.19
3	0.463	<b>0.0069</b>	0.903	<b>50.95</b>	0.0129	0.916	50.83
4	0.481	<b>0.0058</b>	<b>0.945</b>	<b>48.21</b>	0.0187	0.924	48.19
5	0.476	<b>0.0161</b>	0.925	46.47	0.0266	0.934	46.54

method are lower than the errors obtained from WFF+LSPU. Note that the phase errors from WFF+LSPU tend to increase with higher fringe densities at the same noise level, whereas the phase errors from SPUD remain approximately constant regardless of fringe density. Additionally, the errors from SPUD are randomly distributed throughout the phase map, which is a desired property of denoising methods [24], while the errors from

WFF+LSPU are concentrated near high fringe density regions. The quantitative results from Fig. 3 are shown in Table 1 for the three performance metrics. As in the average performance scores, SPUD outperforms WFF+LSPU in terms of phase error  $\sigma_\epsilon$ , and has a comparable performance with respect to WFF+LSPU in terms of  $Q_{index}$  and PSNR. The high  $Q_{index}$  and PSNR values show the restoration capabilities of both methods.

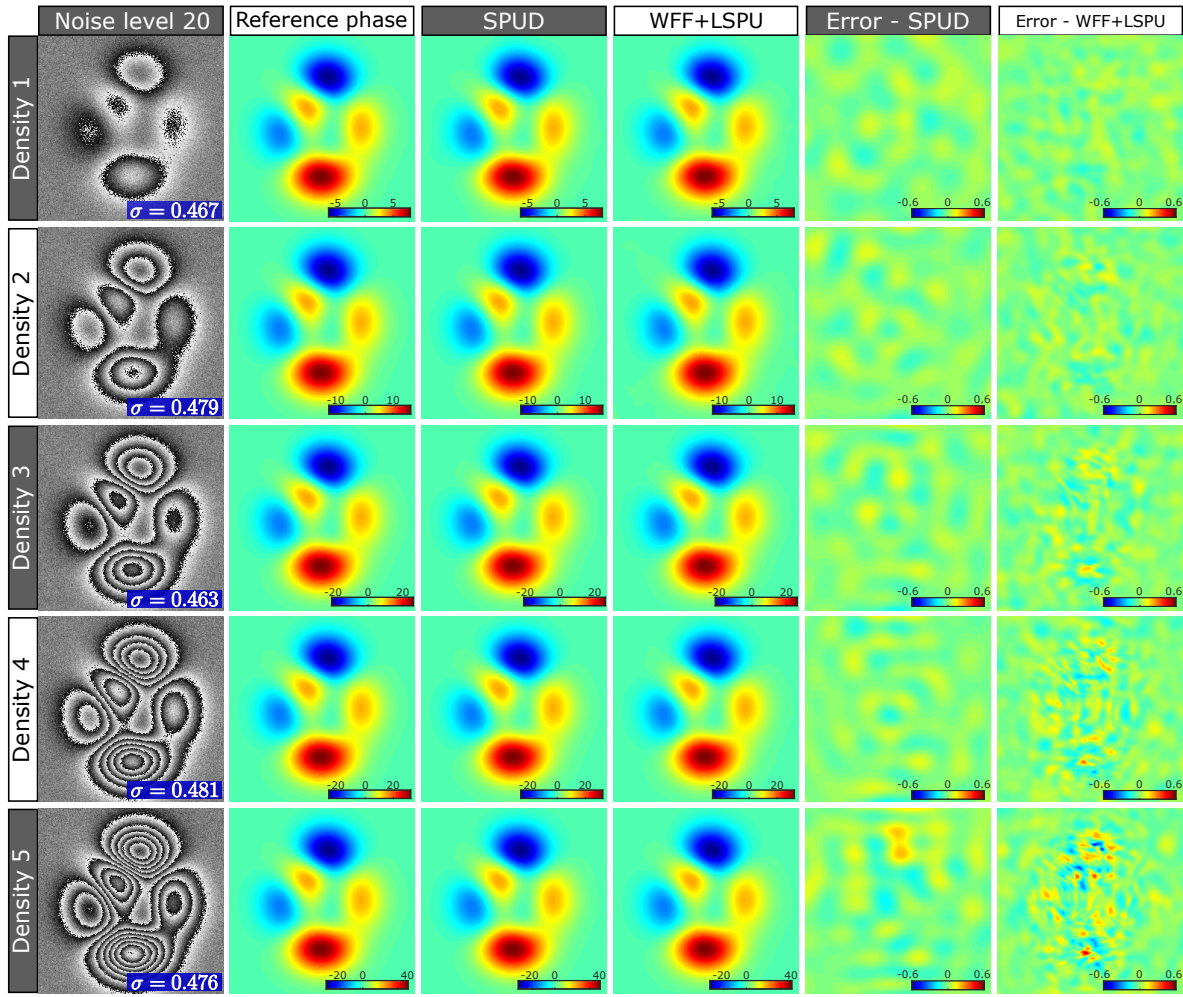


**Fig. 3.** 2D representation of the SPUD and WFF+LSPU performance for the five phase densities and the noise level 20. The SPUD error maps are smoother and the errors are randomly distributed, whereas the WFF+LSPU error maps concentrate high errors in the vicinity of high density fringes.

**Table 2.** Execution time comparison for different array sizes. Time measurements in seconds.

Array Size (pixels)	SPUD (double precision)	WFF+LSPU (double precision)	WFF (GTX295 GPU, single precision)*
256 × 256	0.0069	24.7215	0.25
512 × 512	0.0857	104.2615	0.93
1024 × 1024	0.2326	755.8024	3.60

\* These values are the execution times from processing a fringe pattern image of the same size with WFF, as reported in Ref. [45].

#### D. Execution time assessment

From the above experiments, it can be concluded that the SPUD method obtains a comparable result with WFF+LSPU. However,

the main advantage of the proposed method is its low computational complexity. To illustrate that, we evaluate the execution time of SPUD and WFF+LSPU on a personal computer (PC) with Windows 7 (2.4 GHz i7 intel processor, 8 GB RAM) and MATLAB R2017a. In this experiment, we use three phase maps with the same phase density and noise level, but with different sizes (number of pixels). In Table 2 we show the execution time results for both methods in the phase restoration of array sizes: 256 × 256, 512 × 512, and 1024 × 1024. It can be noted that WFF+LSPU is several orders of magnitude slower than SPUD, and this is mainly due to the high complexity in the denoising stage with WFF. However, since there are GPU implementations of WFF, we include the execution times for the processing of fringe patterns of the same size as reported in Ref. [45]. Even in this scenario, the non-optimized MATLAB implementation of the proposed method in double precision (that includes denoising and unwrapping) is one to two orders of magnitude faster than the GPU implementation of WFF in single precision (only the denoising stage without unwrapping).

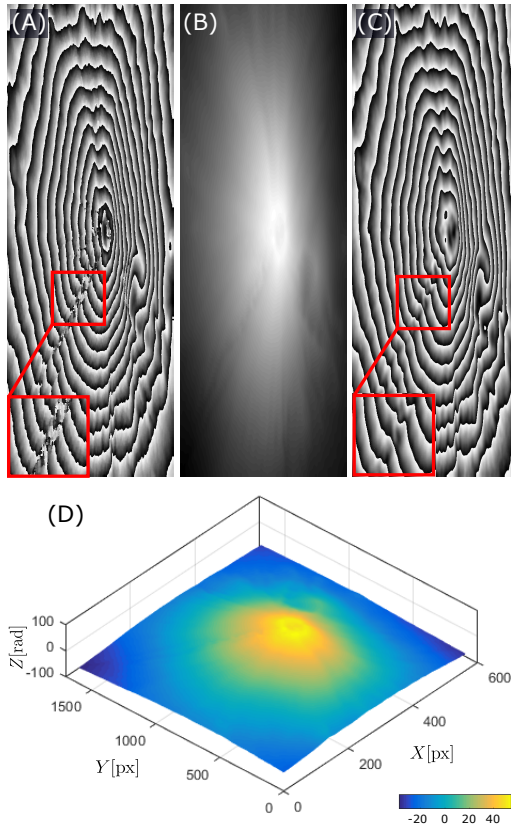


**Fig. 4.** Phase unwrapping by SPUD from an interferometric wrapped phase of size  $1591 \times 561$  pixels. (A) Wrapped phase. (B) Unwrapped phase. (C) Re-wrapped values of the unwrapped phase compared with (A). (D) Mesh of the unwrapped phase. The red box indicates a region of phase dislocations, with a zoomed view.

## 5. EXPERIMENTAL RESULTS

We evaluated the SPUD algorithm on two wrapped phases from InSAR provided as open-source data in Refs. [47, 48]. In Fig. 4(A), we show the first interferometric phase of size  $561 \times 1591$  pixels, which corresponds to the shape of a volcano. Note that the phase map contains regions of phase dislocations. In this situation, filtering by WFF has proven to be unhelpful [14]. Following the threshold formula, we set  $\lambda = 0.5\sqrt{2\log(MN)}$  for these experiments. In Fig. 4(B), we show the unwrapped and restored phase map obtained by SPUD. Since the dynamic range of the unwrapped result is large, we re-wrap the unwrapped values for visual comparison (Fig. 4(C)), as suggested in Ref. [1]. The proposed algorithm removes the regions of phase dislocations from the restored phase map by the smoothing constraint without increasing the computational complexity. Additionally, the unwrapped solution seems congruent with the original data, and no propagation errors are evident. In Fig. 4(D), we show the mesh of the unwrapped phase. The processing time in this experiment was 0.504 s.

In Fig. 5(A), we show the second wrapped phase map of size  $1065 \times 2032$  pixels, which corresponds to a region over Phoenix, Arizona, USA, scanned by the Canadian satellite system, RADARSAT-2. The phase map describes a complex topographic area and exhibits noise. In Fig. 5(B), we show the

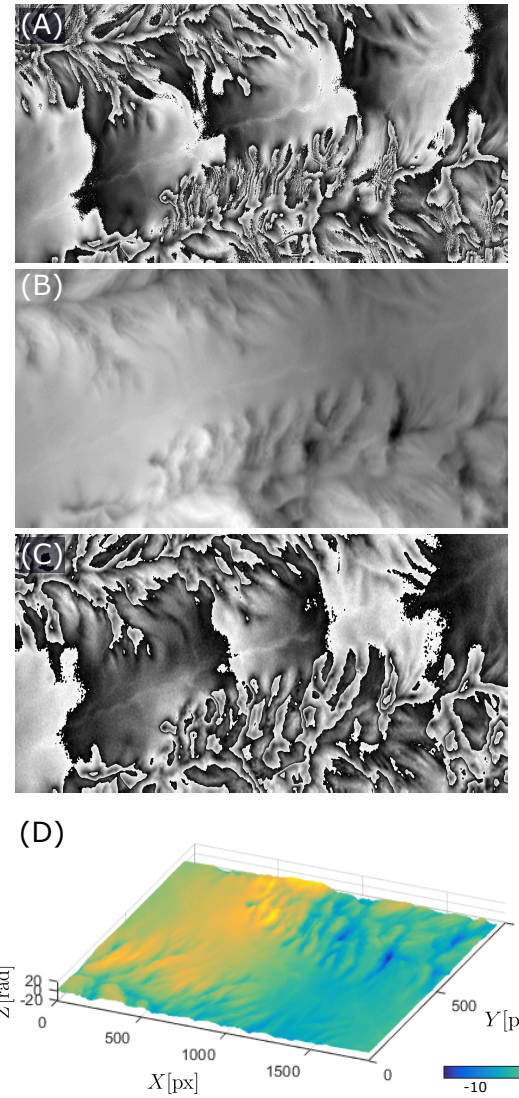


**Fig. 5.** Phase unwrapping by SPUD from an interferometric wrapped phase of size  $1065 \times 2032$  pixels. (A) Wrapped phase. (B) Unwrapped phase. (C) Re-wrapped values of the unwrapped phase compared with (A). (D) Mesh of the unwrapped phase.

unwrapped and restored phase with the proposed method. The re-wrapped phase map is shown in Fig. 5(C). Observe that the effect of noise was minimized with the structural information substantially preserved. The mesh of the unwrapped phase is shown in Fig. 5(D). The processing time for this experiment was 1.04 s.

## 6. CONCLUSION

Phase unwrapping in the presence of noise is a difficult problem, but one that has been traditionally approached from a multi-stage perspective. In this work, we have proposed a method for simultaneous 2D phase unwrapping and denoising based on the least-squares DCT phase unwrapping with an additional sparsity constraint on the DCT coefficients. The proposed method performs better than the state-of-the-art phase denoising method

Windowed Fourier Filtering in terms of phase error, and at par in terms of noise removal. However, the computational complexity of the proposed method is sufficiently low, resulting in several orders of magnitude faster than the benchmark. The processing of experimental data from synthetic aperture radar showed the capability for processing real images, including removing phase dislocations. Future work involves testing the algorithm in other phase retrieval scenarios affected by noise.

## FUNDING

Universidad Tecnológica de Bolívar (UTB) projects C2018P005 and C2018P018.

## DISCLOSURES

The authors declare no conflicts of interest.

## ACKNOWLEDGMENT

J. Pineda and J. Meza thank the Universidad Tecnológica de Bolívar (UTB) for a postgraduate scholarship. L.A. Romero and A.G. Marrugo thank UTB for a Research Leave Fellowship. A.G. Marrugo acknowledges support from the Fulbright Commission in Colombia and the Colombian Ministry of Education within the framework of the Fulbright Visiting Scholar Program, Cohort 2019–2020.

## DATA AVAILABILITY

The final dataset and accompanying code are available on the Code Ocean compute capsule <https://doi.org/10.24433/CO.2865594.v1>.

## REFERENCES

1. D. C. Ghiglia and M. D. Pitts, *Two-dimensional phase unwrapping: theory, algorithms, and software*, vol. 4 (Wiley New York, 1998).
2. H. Yu, Y. Lan, Z. Yuan, J. Xu, and H. Lee, "Phase Unwrapping in InSAR : A Review," *IEEE Geosci. Remote. Sens. Mag.* **7**, 40–58 (2019).
3. J. Bacca, S. Pinilla, and H. Arguello, "Super-resolution phase retrieval from designed coded diffraction patterns," *IEEE Transactions on Image Process.* **29**, 2598–2609 (2020).
4. S. S. Gorthi and P. Rastogi, "Fringe projection techniques: whither we are?" *Opt. lasers engineering* **48**, 133–140 (2010).
5. H. Xia, S. Montresor, P. Picart, R. Guo, and J. Li, "Comparative analysis for combination of unwrapping and de-noising of phase data with high speckle decorrelation noise," *Opt. Lasers Eng.* **107**, 71–77 (2018).
6. M. Zhong, F. Chen, C. Xiao, Y. Yang, and Y. Wei, "Noise reduction in modulation measurement profilometry based on the wavelet transform method," *Opt. Eng.* **57**, 054102 (2018).
7. H. A. Aebsicher and S. Waldner, "A simple and effective method for filtering speckle-interferometric phase fringe patterns," *Opt. Commun.* **162**, 205–210 (1999).
8. R. M. Goldstein, H. A. Zebker, and C. L. Werner, "Satellite radar interferometry: Two-dimensional phase unwrapping," *Radio science* **23**, 713–720 (1988).
9. M. Zhao, L. Huang, Q. Zhang, X. Su, A. Asundi, and Q. Kemao, "Quality-guided phase unwrapping technique: comparison of quality maps and guiding strategies," *Appl. optics* **50**, 6214–6224 (2011).
10. Q. Kemao, W. Gao, and H. Wang, "Windowed fourier-filtered and quality-guided phase-unwrapping algorithm," *Appl. optics* **47**, 5420–5428 (2008).
11. T. J. Flynn, "Consistent 2-d phase unwrapping guided by a quality map," in *IGARSS'96. 1996 International Geoscience and Remote Sensing Symposium*, , vol. 4 (IEEE, 1996), pp. 2057–2059.
12. J. Xu, D. An, X. Huang, and P. Yi, "An efficient minimum-discontinuity phase-unwrapping method," *IEEE Geosci. Remote. Sens. Lett.* **13**, 666–670 (2016).
13. D. C. Ghiglia and L. A. Romero, "Minimum  $l_p$ -norm two-dimensional phase unwrapping," *JOSA A* **13**, 1999–2013 (1996).
14. L. Meng, S. Fang, P. Yang, L. Wang, M. Komori, and A. Kubo, "Image-inpainting and quality-guided phase unwrapping algorithm," *Appl. optics* **51**, 2457–2462 (2012).
15. W. Shi, Y. Zhu, and Y. Yao, "Discussion about the dct/fft phase-unwrapping algorithm for interferometric applications," *Optik* **121**, 1443–1449 (2010).
16. H. Xia, S. Montresor, R. Guo, J. Li, F. Yan, H. Cheng, and P. Picart, "Phase calibration unwrapping algorithm for phase data corrupted by strong decorrelation speckle noise," *Opt. express* **24**, 28713–28730 (2016).
17. J. Pineda, R. Vargas, L. A. Romero, J. Meneses, and A. G. Marrugo, "Fringe Quality Map for Fringe Projection Profilometry in LabVIEW," *Opt. Pura Apl.* **51**, 50302:1–8 (2018).
18. S. Montresor and P. Picart, "Quantitative appraisal for noise reduction in digital holographic phase imaging," *Opt. express* **24**, 14322–14343 (2016).
19. W. K. Pratt, "Generalized wiener filtering computation techniques," *IEEE Transactions on Comput.* **100**, 636–641 (1972).
20. R. C. Gonzalez, R. E. Woods *et al.*, "Digital image processing," (2002).
21. S. Mallat, *A wavelet tour of signal processing* (Elsevier, 1999).
22. D. L. Donoho, "De-noising by soft-thresholding," *IEEE transactions on information theory* **41**, 613–627 (1995).
23. A. Buades, B. Coll, and J.-M. Morel, "A review of image denoising algorithms, with a new one," *Multiscale Model. & Simul.* **4**, 490–530 (2005).
24. A. Buades, B. Coll, and J.-M. Morel, "Non-local means denoising," *Image Process. On Line* **1**, 208–212 (2011).
25. A. Buades, B. Coll, and J.-M. Morel, "A non-local algorithm for image denoising," in *2005 IEEE Computer Society Conference on Computer Vision and Pattern Recognition (CVPR'05)*, , vol. 2 (IEEE, 2005), pp. 60–65.
26. K. Dabov, A. Foi, V. Katkovnik, and K. Egiazarian, "Image denoising with block-matching and 3d filtering," in *Image Processing: Algorithms and Systems, Neural Networks, and Machine Learning*, , vol. 6064 (International Society for Optics and Photonics, 2006), p. 606414.
27. K. Dabov, A. Foi, V. Katkovnik, and K. Egiazarian, "Image denoising by sparse 3-d transform-domain collaborative filtering," *IEEE Transactions on image processing* **16**, 2080–2095 (2007).
28. Q. Kemao, "Windowed fourier transform for fringe pattern analysis," *Appl. Opt.* **43**, 2695–2702 (2004).
29. Q. Kemao, "Two-dimensional windowed fourier transform for fringe pattern analysis: principles, applications and implementations," *Opt. Lasers Eng.* **45**, 304–317 (2007).
30. P. Memmolo, I. Esnaola, A. Finizio, M. Paturzo, P. Ferraro, and A. Tulino, "Spadedh: a sparsity-based denoising method of digital holograms without knowing the noise statistics," *Opt. Express* **20**, 17250–17257 (2012).
31. P. Memmolo, M. Iannone, M. Ventre, P. A. Netti, A. Finizio, M. Paturzo, and P. Ferraro, "Quantitative phase maps denoising of long holographic sequences by using spadedh algorithm," *Appl. optics* **52**, 1453–1460 (2013).
32. J. P. Krishnan, M. A. Figueiredo, and J. M. Bioucas-Dias, "Sure-fuse wff: A multi-resolution windowed fourier analysis for interferometric phase denoising," *IEEE Access* (2019).
33. H. Xia, S. Montresor, R. Guo, J. Li, F. Olchewsky, J.-M. Desse, and P. Picart, "Robust processing of phase dislocations based on combined unwrapping and inpainting approaches," *Opt. letters* **42**, 322–325 (2017).
34. J. L. Marroquin and M. Rivera, "Quadratic regularization functionals for phase unwrapping," *JOSA A* **12**, 2393–2400 (1995).
35. L. Guerriero, G. Nico, G. Pasquariello, and S. Stramaglia, "New regularization scheme for phase unwrapping," *Appl. Opt.* **37**, 3053–3058 (1998).

36. L. Zhou, D. Chai, Y. Xia, P. Ma, and H. Lin, "Interferometric synthetic aperture radar phase unwrapping based on sparse markov random fields by graph cuts," *J. Appl. Remote. Sens.* **12**, 015006 (2018).
37. X. Wang, Z. Zhang, Z. Guo, and H. Wang, "Study on the unweighted least-squares phase unwrapping algorithm," in *Holography, Diffractive Optics, and Applications IV*, , vol. 7848 (SPIE, 2010), p. 784830.
38. J. C. Estrada, M. Servin, and J. A. Quiroga, "Noise robust linear dynamic system for phase unwrapping and smoothing," *Opt. express* **19**, 5126–5133 (2011).
39. G. Yu and G. Sapiro, "Dct image denoising: a simple and effective image denoising algorithm," *Image Process. On Line* **1**, 292–296 (2011).
40. D. L. Donoho and J. M. Johnstone, "Ideal spatial adaptation by wavelet shrinkage," *biometrika* **81**, 425–455 (1994).
41. J. M. Bioucas-Dias and G. Valadão, "Phase Unwrapping via Graph Cuts," *Image Process. IEEE Transactions on* **16**, 698–709 (2007).
42. H. Hongxing and W. Lingda, "PUMA-SPA: A Phase Unwrapping Method Based on PUMA and Second-Order Polynomial Approximation," *IEEE Geosci. Remote. Sens. Lett.* **11**, 1906–1910 (2014).
43. O. Dalmau, M. Rivera, and A. Gonzalez, "Weighted robust basis function for phase unwrapping," *Opt. Lasers Eng.* **69**, 13–19 (2015).
44. T. Zhang, S. Jiang, Z. Zhao, K. Dixit, X. Zhou, J. Hou, Y. Zhang, and C. Yan, "Rapid and robust two-dimensional phase unwrapping via deep learning," *Opt. express* **27**, 23173–23185 (2019).
45. W. Gao, N. T. T. Huyen, H. S. Loi, and Q. Kemao, "Real-time 2D parallel windowed Fourier transform for fringe pattern analysis using Graphics Processing Unit," *Opt. express* **17**, 23147–23152 (2009).
46. Z. Wang, A. C. Bovik, and L. Lu, "Why is image quality assessment so difficult?" in *2002 IEEE International Conference on Acoustics, Speech, and Signal Processing*, , vol. 4 (IEEE, 2002), pp. IV–3313.
47. F. J. Hernandez-Lopez, M. Rivera, A. Salazar-Garibay, and R. Legarda-Sáenz, "Comparison of multihardware parallel implementations for a phase unwrapping algorithm," *Opt. Eng.* **57**, 043113 (2018).
48. SAR-EDU, "Sar-edu remote sensing education initiative, dem generation with matlab," (2019).